Tandem process for in situ H_2O_2 formation coupled with benzyl alcohol oxidation by Pd-Au bimetallic catalysts.

Jordan Santiago Martinez,[a] Jaime Mazarío,[a] Silvia Gutiérrez-Tarriño,[a] Carmen Galdeano-Ruano,[a] José Gaona-Miguélez,[a] Marcelo E. Domine,[a] and Pascual Oña-Burgos*[a,b]

[a] *Instituto de Tecnología Química (ITQ) Universitat Politécnica de Valencia-CSIC, Av. de los Naranjos - s/n 46022 Valencia, Spain.*

[b] *Department of Chemistry and Physics, Research Centre CIAIMBITAL, University of Almería, Ctra. Sacramento, s/n, 04120 Almería, Spain.*

Abstract

Alcohol oxidation is among the most important industrial organic reactions. Traditionally, the best-suited catalysts are Pd, Pt and Au supported nanoparticles. The research community has recently started drawing-up strategies to synthesize carbon-supported Pd/Au bimetallic nanoparticles (NPs), leading to higher activities and selectivities. However, metallic active species in these catalysts are usually generated by using sodium borohydride ($NaBH_4$), which is not synthetically easy to reproduce. In fact, minor modifications in pH, concentration and/or other parameters have a prominent effect on the nature of the promoted material. In this work, a robust process involving dihydrogen flow (H_2) at 200 °C as a reducing agent to synthesize Pd/Au supported bimetallic materials was considered an alternative to the common pathway. Discussions on structural and physicochemical properties of materials from different reducing reagents and composition ranges were developed using HR-TEM, XRD, CO chemisorption, and XPS. Their stability and activity were also tested on benzyl alcohol oxidation to benzaldehyde under mild reaction conditions (60 °C, water as solvent, and P_{O_2} = 1.5 bar). Noticeably, a catalyst from the hydrogen reduction process with a metal composition of 0.8%Pd-0.2%Au/C consisting of bimetallic clusters (≈ 1.5 nm) proved to be the best material (C = 94%, S = 99%). Catalytic performances were strongly correlated with structural properties, such as nanoparticle size and distribution, which, in turn, were affected by the reduction step and the metal composition range. Finally, the oxidant influence in the benzyl alcohol oxidation has also been studied, along with a first approach for the tandem *in situ* formation of H_2O_2 coupled with alcohol oxidation.

1. Introduction

The oxidation of benzyl alcohol is a common-used model reaction for the selective oxidation of alcohols, due in part to the limited number of products and the relatively well-known pathways for their formation.[1] In addition, the oxidation of benzyl alcohol to benzaldehyde is significant in its own right, since the latter is used in the perfumery, dye and agrochemical industries.[2] Among all known developed catalytic methods, the oxidation of benzyl alcohol with clean oxidants such as hydrogen peroxide or molecular oxygen using heterogeneous catalysts represents the most sustainable one.[3–5] The main advantage of this method is the generation of only one by-product: water. Consequently, there is a current scientific effort concerning developing a selective heterogeneous catalyst for this process using clean oxidants. In this sense, various systems such as hydrotalcites,[6] heteropoly-acids[7] or mixed metal oxides[8,9] able to perform the selective alcohol dehydrogenation have been proved to have enough chemical and thermal stability. However, considering reactants accessibility to active sites and metal leaching from solid supports, the most relevant materials designed up to now are metal nanoparticles such as Co, Ir, Pt, Pd or Au supported on different materials (metal oxides or carbon).[2,3,7,10–15] This kind of catalytic system promotes an enhancement of the contact between the reagents and catalytic centers mainly induced by the higher surface area of the support and, therefore, the higher dispersion of the active phase. Concretely, many of the active catalysts reported in the literature for this reaction contain typically bimetallic nanoparticles consisting of Au and Pd.[11,16–18] In this regard, an increase in benzyl alcohol conversion have been observed with bimetallic catalysts, compared with the monometallic ones, together with high selectivity to benzaldehyde with limited overoxidation to benzoic acid.[9,10,19]

Interestingly, this kind of Pd-Au bimetallic nanoparticles has been extensively studied by several independent research groups such as Hutchings,[13,20] Goodman[19] and Ishihara[21] for H_2O_2 production from H_2 and O_2. In principle, the reaction between hydrogen and oxygen is the simplest method to form hydrogen peroxide. Taking into account that the main problem for the use of hydrogen peroxide as an oxidant at a large scale is safe transporting and storage,[20] the *in situ* generation and successive utilization of this oxidant could be a great alternative, ideally with the use of a single catalyst for both reaction steps.

In that sense, some works in the literature report Pd-Au bimetallic nanoparticles that are active for both reactions.[20,22,23] However, the synthesis procedures of these bimetallic catalysts usually involve sodium borohydride as a reductive agent.[24,25] For these reasons, the main goal of this work is to synthesize supported single-phase bimetallic nanoparticles based on gold and palladium in a more sustainable way, involving hydrogen as a reductive agent, for the

selective oxidation of benzyl alcohol using *in situ* generated hydrogen peroxide as oxidant. For this purpose, first, bimetallic Pd-Au nanoparticles have been synthesized through two different methods and with different Pd/Au ratios to study the influence of the reductive agent and the metal ratio in the activity and selectivity of the obtained materials in the benzyl alcohol oxidation (Scheme 1). Furthermore, this reaction has been carried out using different oxidants and catalysts with different Au/Pd ratios to correlate the influence of each metal loading and the nature of the oxidant on the catalytic process. The best catalysts of this work have been tested in hydrogen peroxide production and the one-pot benzyl alcohol oxidation coupled with *in situ* hydrogen peroxide production. Finally, all catalysts obtained have been exhaustively characterized to determine their structural and physicochemical properties, as well as to identify the active centers and their accessibility, thus correlating their structure with the catalytic activity.

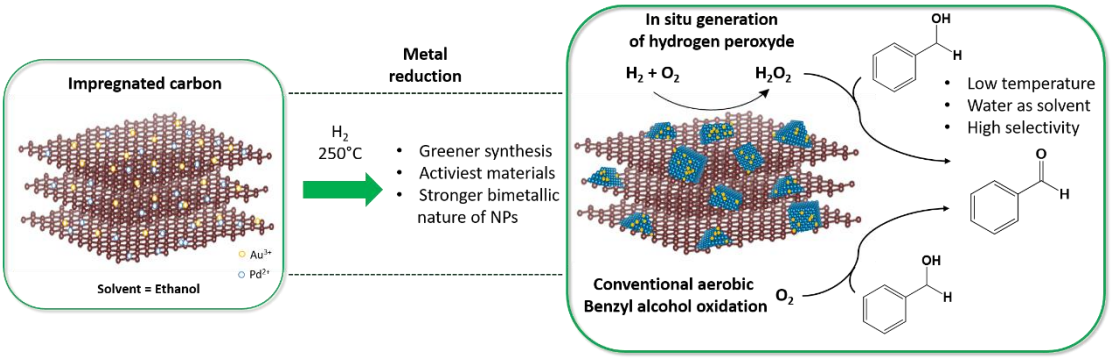

Scheme 1. Resume of the studied process.

2. Experimental Section

2.1.Materials

Sodium tetrachloroaurate (III) dihydrate ($NaAuCl_4.2H_2O$, 99%), PolyVinylAlcohol ($(C_2H_4O)_n$ Mw = 89000-98000 g/mol, 99% hydrolyzed), Sodium borohydride ($NaBH_4$, 99%), Sodium tetrachloropalladate (II) (Na_2PdCl_4, 98%) and Gold chloride (III) ($AuCl_3$, 99%) were purchased from Sigma Aldrich and Activated Carbon Vulcan XC72R from Cabot.

2.2.Catalyst preparation

Synthesis of Pd-Au-NBH catalyst supported on carbon.

The catalysts named **xPd-yAu-NBH** (x the wt% of Pd and y the wt% of Au) were synthesized following a reported method.[26] Briefly, the synthesis consists of preparing a gold salt aqueous solution in the presence of PVA. The metal is reduced by an aqueous solution of $NaBH_4$ and the resulting colloidal solution is then acidified until pH = 2. Once the reduction step is completed, the activated carbon is added, and the slurry is vigorously stirred for 2h. The material is recovered by vacuum filtration and dried overnight at 100 °C. Finally, the previous

step is repeated with Palladium instead of Gold in order to obtain the desired catalyst. (See SI Appendix A for more details).

Synthesis of Pd-Au-H catalyst supported on carbon (H_2-reduction methodology).

The catalysts named **xPd-yAu-H** (x the wt% of Pd and y the wt% of Au) were synthesized through a new greener approach, choosing H_2 instead of $NaBH_4$, as the reducing agent. For example, **0.2Pd-0.8Au-H**, 0.012 mmol (3.6 mg) of Na_2PdCl_4 and 0.024 mmol (9.53 mg) of $NaAuCl_4 \cdot 2H_2O$ were dissolved and stirred in 50 mL of ethanol for 12 hours. Then, 300 mg of activated carbon Vulcan XC72R were added and vigorously stirred overnight under a nitrogen atmosphere. The flask was wrapped in aluminum paper to avoid photo-reduction. Finally, the solvent was removed under vacuum. The resulting dried powder was then reduced during 2h at 200 °C under a hydrogen flow (gradient temperature 3 °C/min and hydrogen flow = 100 mL/min). Finally, a nitrogen flow was passed until room temperature (40 mL/min).

2.3. Oxidation experiments

The reactions were carried out in a 6 mL glass microreactor, equipped with a pressure-gauge and a metallic probe for sample collection, on a thermostatic hotplate coupled with a magnetic stirrer (1400 rpm). Alcohol (0.3 mol/L) and catalyst (substrate/metal: 500:1 mol ratio) were mixed in distilled water (total volume of 2 mL). The reactor was then pressurized at the desired oxygen pressure and/or hydrogen peroxide was added (13 µL/h). Then, the reaction was heated at 60 °C and stirred (1400 rpm) during the corresponding time. Once the reaction was finished, the catalyst was removed by vacuum filtration and the products were then extracted from the filtrate with toluene. Products were identified and analyzed by gas chromatography (Figure S2) (Agilent 7890A equipped with HP5 column: 32 m, 0.25 mm/0.25 µm). Reactant conversion and product quantification were determined from GC data using calibration curves using dodecane as internal standard (Scheme 2):

$$Conversion\ (\%) = \frac{initial\ mol\ of\ reactant - finalmol\ \ of\ reactant}{mol\ initial\ of\ reactant} \times 100$$

$$Selectivity\ (\%) = \frac{mol\ of\ desired\ product}{mol\ of\ converted\ reactant} \times 100$$

$$TON\ (Turnover\ Number) = \frac{mol\ of\ consumed\ reactant}{mol\ of\ metal\ in\ the\ catalyst}$$

$$TOF\ (Turnover\ Frequency\ h^{-1}) = \frac{TON}{Time}$$

Scheme 2. Equations for the calculation of different parameters.

2.4. In situ generation of H_2O_2 and benzyl alcohol oxidation

In situ hydrogen peroxide production was performed in a 20 mL glass vessel inside a stainless-steel reactor. 5 mg catalyst were deposited in the vessel together with 4000 mg of ultrapure water. The reactor was sealed, leak tested and purged with nitrogen. After that, it was placed inside a cooling system with magnetic stirring at 1000rpm and pressurized with 30 bar of CO_2. When the reactor reached a temperature of 0 ºC and the pressure inside dropped from 30 to 20 bar, 10 bar of H_2 were added. The initial point of the reaction was considered the addition of 10 bar of O_2. At this point, a pressure of 40 bar is reached. 100uL of benzyl alcohol is then introduced into the reactor. In order to monitor the hydrogen peroxide concentration, samples of 50 µL were taken and put into a vial filled with 1 mL of acetone, 10 µL of decane as standard, and 100 µL of a 10% triphenylphosphine solution (Scheme 3) in acetone and analysed by gas chromatography (Agilent 7890A equipped with HP5 column: 32 m, 0.25 mm/0.25 µm). In this case, the conversion and selectivity were calculated by NMR ^1H experiments in $CDCl_3$. (Figure S9-S12)

$$H_2O_2 + Triphenylphosphine \longrightarrow H_2O + Triphenylphosphine\ oxide\ (TFFO)$$

$$nH_2O_2 = nTFFO = \frac{nInternalStandard \times Area\ TFFO}{response\ factor TFFO \times Area\ Internal\ standard}$$

Scheme 3. Equations for the calculation of generated H_2O_2.

2.5 Catalyst characterization

Scanning Transmission Electron Microscopy (STEM). STEM images of catalysts and EDX studies were carried out using a JEOL electron microscope Model 2100F with an operating voltage of 200 kV. Samples were dispersed in dichloromethane under sonication. A few drops of the suspension were poured onto a carbon-coated copper grid and dried at room temperature. Measurements were set up using Annular Dark field. Using this technique, the shape, size, and dispersity of nanoparticles on carbon could be observed. In this sense, more than 200 particles were measured by using an image analyzer software (ImageJ). Then, relative frequency distributions with a gaussian fitting were set up on size values to estimate each material's average particle size. Moreover, Energy Dispersive X-Ray (EDX) analysis was recorded to assess the metal nanoparticle composition.

Powder X-ray diffraction (XRD). Powder X-ray diffraction was carried out with a HTPhilips X'Pert MPD diffractometer equipped with a PW3050 goniometer using Cu Kα radiation and a multisampling handler at a scan rate of 2 min^{-1}, operating at 40 kV and 35 mA, provided with a variable divergence slit and working in fixed irradiated area mode. Crystalline phases were identified using the Joint Committee on Powder Diffraction Standards database (JCPDS).

CO chemisorption. CO chemisorption isotherms were carried out in an ASAP 2010C equipment at 308 K. Before starting the adsorption, the samples (ca. 0.250 g) were pre-treated in H_2 at 200 ºC for 2 h and stabilized under vacuum for 30 min. After reduction, samples were degassed at 1333 x 10^{-3} Pa during 2 h at 400 ºC, and then, temperature lowered at 35 ºC. Next, pure CO was admitted and the first adsorption isotherm (i.e. the total CO uptake) was measured. After evacuation at 35 ºC, the second isotherm (i.e. the reversible CO uptake) was taken. The amount of chemisorbed CO was calculated by subtracting the two isotherms. Assuming any fixed stoichiometry CO: Pd might be considered purely speculative, values are also provided for mol of CO absorbed per gram of catalyst.

X-ray photoelectron spectroscopy (XPS). XPS spectra were obtained at room temperature with a SPECS spectrometer equipped with a Phoibos 150MCD-9 analyzer and using nonmonochromatic MgKα (1253.6 eV) operating at 100 W. The XPS regions were recorded at 30 eV pass energy with a step size of 0.1 eV and operating pressure of 10^{-9} mbar. Intensities were corrected by the transmission function of the spectrometer. Gaussian-Lorentzian (Voigt) curves together with a nonlinear-Shirley (*Au4f, Pd3d, O1s*) and a U2 Tougaard (*C1s*) background subtraction were used for curve fitting. During data processing of the XPS spectra, the binding energies (B.E.) of all photoelectron lines were calibrated to the *C1s* photopeak position at 284.3 eV, corresponding to graphitic carbon. CASAXPS software was used for spectra treatment and quantification.[27]

The corresponding amounts of Pd and Au deposited in the catalysts are determined by the loss of metal in precursors solutions measured by ICP (see more details in SI).

3. Results and discussion

3.1 Synthesized catalysts and preliminary catalytic tests

In this work, two different methodologies were used to synthesize bimetallic Au-Pd nanoparticles. First is the conventional one, in which $NaBH_4$ is used as a reducing agent. From this methodology, were obtained the catalysts denoted as **xPd-yAu-NBH**, where ***x*** represents Pd weigth percentage, ***y*** represents Au weight percentage and **NBH** represents the reducing agent. The second methodology consists of using H_2 as a reducing agent. From this methodology, catalysts were obtained denoted as **xPd-yAu-H**, where again ***x*** represents Pd weight percentage, ***y*** represents Au weight percentage and **H** represents the reducing method (more information in the experimental section). In addition, several materials have been synthesized to study the influence of the metal ratio in Au-Pd bimetallic catalysts, changing this parameter. All synthesized and studied materials are summarized in Table 1. Furthermore,

1.00Pd-H and **1.00Au-H** have been synthesized as reference materials to prove the synergistic effect between gold and palladium.

First, the synthesized catalysts were tested on aerobic benzyl alcohol oxidation, as a preliminary test. The catalytic activity of these catalysts in this primary alcohol reaction was compared after 6h of reaction time, being quantified the alcohol conversion and the aldehyde selectivity. In addition, benzoic acid was the only detected by-product. According to Table 1, the gold catalyst does not present any catalytic activity for primary alcohol oxidation. At first, this observation was not expected because literature depicted another behavior toward alcohol oxidation when using this kind of catalyst.[28–30] However, literature has already explained that Au cannot catalyse the rate-limiting alcohol dehydrogenation step in the absence of a strong base.[31,32] Contrary to the gold catalyst, the pure palladium catalyst shows a significant benzyl alcohol conversion into benzaldehyde (C = 84%, S = 99%).

Table 1. Benzyl alcohol oxidation for different catalysts.[a]

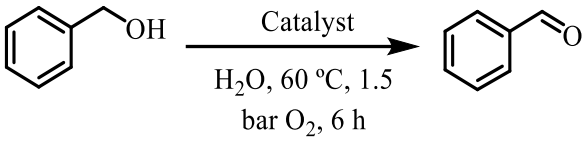

Catalyst	Composition (wt%)[b]	Conversion (%)	Selectivity (%)[c]
1.00Pd-NBH	1.00%Pd/C	20	96
0.8Pd-0.2Au-NBH	0.80%Pd-0.20%Au/C	26	98
0.5Pd-0.5Au-NBH	0.50%Pd-0.50%Au/C	80	97
0.2Pd0.8Au-NBH	0.20%Pd-0.80%Au/C	42	96
1.00Au-NBH	1.00%Au/C	0	0
1.00Pd-H	1.00%Pd/C	84	99
0.8Pd-0.2Au-H	0.80%Pd-0.20%Au/C	95	90
0.5Pd-0.5Au-H	0.50%Pd-0.50%Au/C	99	72
0.2Pd-0.8Au-H	0.20%Pd-0.80%Au/C	75	97
1.00Au-H	1.00%Au/C	0	0

[a]Reaction conditions: [benzyl alcohol] = 0.3M, alcohol/metal ratio: 500/1 mol, 60 °C, 1.5 bar O_2, 6 h. [b]Experimental mass introduced during the synthesis. [c]Benzoic acid was the only detected by-product. Carbon balances were above 90% in all cases.

In addition, bimetallic catalysts and, particularly, those synthesized with hydrogen as a reducing agent, present the best activities for this specific reaction. In fact, **0.8Pd-0.2Au-H**

gives the highest activity among all tested catalysts (C = 95%, S = 90%). With this observation, and by comparing **1.00Pd-H**, **1.00Au-H,** and **0.8Pd-0.2Au-H**, the synergistic effect between Au-Pd previously depicted in the introduction is observable. Nevertheless, another bimetallic catalyst such as **0.2Pd-0.8Au-H** shows less activity than the monometallic one. Therefore, it is also true that the metal ratio of this bimetallic system should also partially account for an effect on the catalytic performance. Therefore, from these preliminary results, it seems that the most promising catalyst in Table 1 is **0.8Pd-0.2Au-H.**

3.2 Characterization results

In a first approximation, Scanning Transmission Electron Microscopy (STEM) and energy-dispersive X-ray spectroscopy (EDX) investigations were conducted to understand in more detail the remarkable activity difference between the synthesized catalysts. STEM images of all catalysts were acquired (Figure 2). The comparison between **0.8Pd-0.2Au-NBH** (Figure 1.) and **0.8Pd-0.2Au-H** (Figure 1.) can be used as evidence of the differences generated by the two reduction procedures used during the catalyst syntheses. In a first instance, each sample revealed the presence of nanoparticles supported on carbon. **0.8Pd-0.2Au-NBH**, **0.8Pd-0.2Au-H** present an average particle size of 5.8 ± 2.0 nm and 1.4 ± 0.3 nm, respectively (the particle size of other catalysts with different metal ratios are given in Figure 2). From these results, it can be observed that particle size is smaller for **0.8Pd-0.2Au-H** than for **0.8Pd-0.2Au-NBH**. This finding indicates that hydrogen reduction is more suitable than $NaBH_4$ reduction in order to downsizing nanoparticles to clusters, which is even further confirmed when all the average particle sizes are compared. In addition, the standard deviation from the Gaussian fitting was analyzed, and the particle size in hydrogen reduced catalysts turned out to be more homogeneous than in sodium borohydride reduced catalysts. The better ability of H_2 to penetrate through a hydrophobic material can probably be the reason behind a more effective uniform nucleation of the nanoparticles.[33] Moreover, Figure 1b and 1e show measured nanoparticle plane distances of **0.8Pd-0.2Au-H** (2.30 Å corresponding to (111) plane of PdAu NPs) and **0.8Pd-0.2Au-NBH** (2.24 Å corresponding to (111) plane of Pd NPs) respectively. These results suggest a stronger bimetallic nature of the nanoparticles synthesized by the hydrogen reduction process than those prepared by sodium borohydride reduction method.

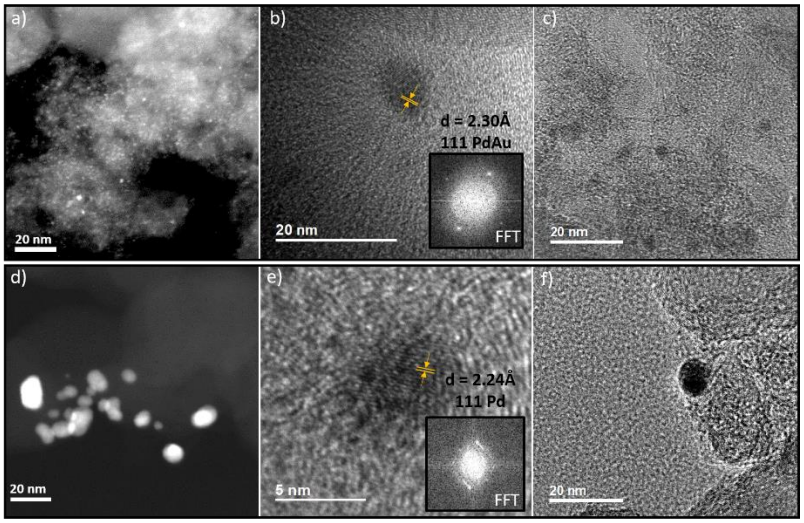

Figure 1. a) STEM images, b), c) TEM images with measured interplanar distance of **0.8Pd-0.2Au-H.** d) STEM images, e), f) TEM images with measured interplanar distance of **0.8Pd-0.2Au-NBH.**

On the other hand, the **1.00Pd-H** catalyst shows a histogram where two maxima are noticeable (Fig. 2f), remaining only that one corresponding to small particle sizes when gold is introduced in the synthesis. This fact probably points to two different crystallization mechanisms in the absence of gold. Thus, another remarkable conclusion that can be drawn from this STEM imaging is that the introduction of Au in the catalysts synthesized by using H_2 as the reducing agent directs the crystallization towards a mechanism leading only to small clusters.

Since the most interesting catalyst, based on the catalytic behavior, appear to be **0.8Pd-0.2Au-H**, EDX analysis coupled with the STEM measurement was carried out (Figure S3). It revealed the presence of gold and palladium in the same nanoparticle**.** Thus, at this point, the new proposed synthesis with hydrogen reduction can be considered suitable for obtaining bimetallic and small carbon-supported PdAu nanoparticles.

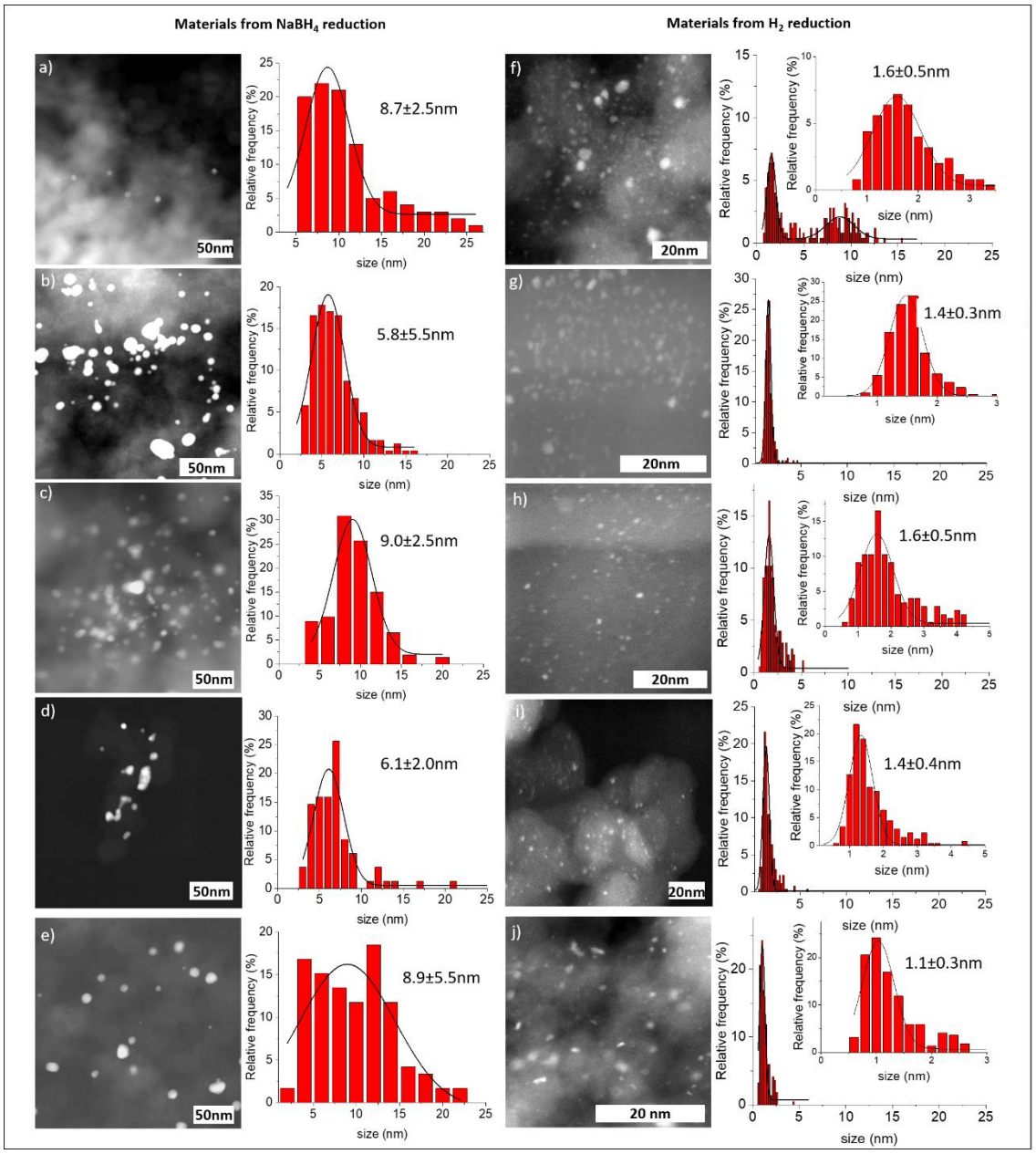

Figure 2. STEM images and the corresponding NPs size distribution fitted by gaussian function. a) **1.00Pd-NBH**, b) **0.8Pd-0.2Au-NBH**, c) **0.5Pd-0.5Au-NBH**, d) **0.2Pd-0.8Au-NBH**, e) **1.00Au-NBH**, f) **1.00Pd-H**, g) **0.8Pd-0.2Au-H**, h) **0.5Pd-0.5Au-H**, i) **0.2Pd0.8Au-H**, j) **1.00Au-H**, respectively. A minimum number of 200 NPs has been considered in all the studied samples.

This fact has also been corroborated by CO-Chemisorption measurements, which were set up on 3 different catalysts (Table S1). The obtained results show that the catalysts present a higher dispersion of the Pd-Au alloy when prepared by the thermal reduction with hydrogen, which also increases when the composition is adequately optimized (**0.8Pd-0.2Au-H**). Obviously, all these observations might have important effects on the catalytic performance of the obtained catalysts, as will be discussed in the next sections.

In addition, X-ray powder diffraction was also used to identify the synthesized materials' crystalline phases. The XRD for those catalysts reduced by dihydrogen or sodium borohydride were considered (Figure 3). The idea was to observe a potential variation in the crystalline phases with the incorporation of gold. Indeed, by either introducing gold in palladium or palladium in gold structures, the interatomic distance could change so that the lattice constant parameter could change too and the presence of bimetallic nanoparticles might be proved.[34] Firstly, patterns were indexed according to the JCPDS cards of palladium and gold (Table S2). The two metals crystallize in a cubic face-centered mode and, therefore, they present the same reticular planes. The most relevant planes for this discussion are (200), (220) and (311). For the **1.00Au-H** pattern shown in Figure 3, (200), (220) and (311) planes are well defined. However, in the presence of palladium, the signals corresponding to these facets for hydrogen reduced materials shifts towards higher angles, becoming positionally closer to the ones exhibited by **1.00Pd-H**. As previously reported, this is proof of the bimetallic nanoparticle formation,[35,36] and it can be explained by the introduction of gold in the palladium lattice. In order to confirm this fact, experimental and theoretical lattice constant parameters have been calculated for different composition range (Table S2). When we focused on the variation of this parameter as a function of palladium content (Figure S4), the experimental tendency is very close to the theoretical one (-0.00165 experimental vs -0.00194).

In the case of those catalysts reduced by sodium borohydride (Figure 3), XRD patterns are similar to hydrogen-reduced catalysts, although some differences can be noticed. Concerning the nature of nanoparticles, no facet shifts have been detected, suggesting a monometallic nature of the nanoparticles. Moreover, peak intensities from metal planes are greater than for hydrogen reduced catalysts. Considering the Debye-Scherrer relation,[37] this phenomenon reveals the presence of larger nanoparticles, in agreement with STEM results. Finally, a peak of an impurity at ≈ 33°, corresponding to the (200) plane of solid palladium oxide (JCPDS n°98 000 9665, detected for the catalysts synthesized through the H_2 reduction method, is not detected in the case of sodium borohydride reduced catalysts.

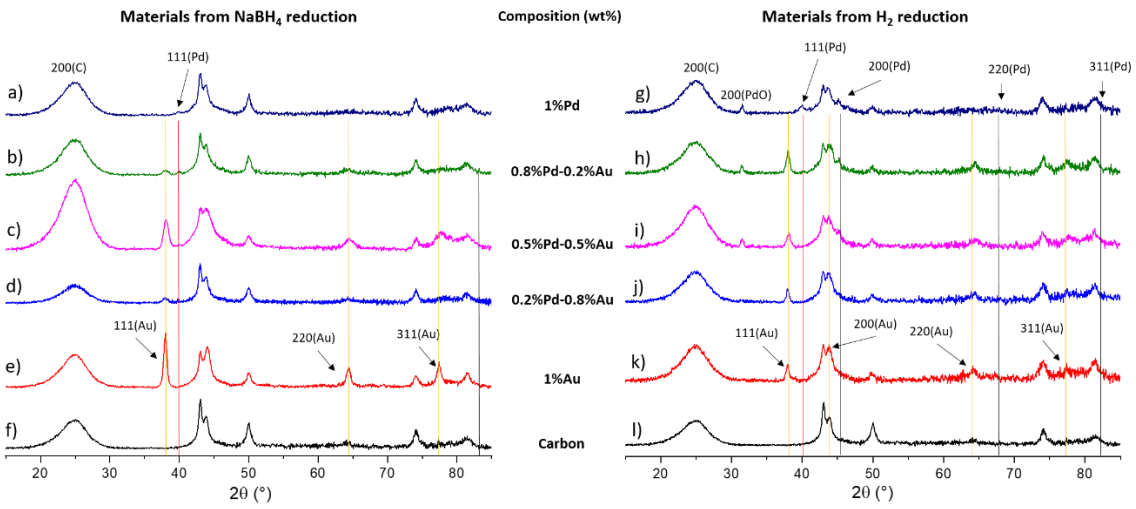

Figure 3. XRD patterns of sodium borohydride reduced catalysts: a) **1.00Pd-NBH**, b) **0.8Pd-0.2Au-NBH**, c) **0.5Pd-0.5Au-NBH**, d) **0.2Pd-0.8Au-NBH**, e) **1.00Au-NBH;** and XRD patterns of dihydrogen reduced catalysts: g) **1.00Pd-H**, h) **0.8Pd-0.2Au-H**, i) **0.5Pd-0.5Au-H**, j) **0.2Pd-0.8Au-H**, k) **1.00Au-H**, f) and l) correspond to XRD of Activated Carbon Vulcan XC72R.

With the aim of gaining further insight into the electronic structure of the elements in the nanoparticles, X-ray photoelectron spectroscopy was carried out for **0.8Pd-0.2Au-H**, the best catalyst of this work, and for **1.00Pd-H** and **1.00Au-H**, to use them as a reference. Theoretically, as it is widely used for in the recent literature,[38,39] XPS enables the detection of electronic modification upon the formation of bimetallic alloys.

First, the highly oriented graphitic nature of the carbonaceous support herein used (VULCAN XC72R) made a careful fitting and interpretation of the C*1s* region necessary to obtain a reliable reference for charge correction (Figure S5a),[40] whose value has been fixed at 284.3 eV and ascribed to C-C (sp^2, graphitic carbon). The result of this fitting is in good agreement with what other authors recently reported for this material,[41] and it has been extended to C*1s* regions in the other samples. Regarding Pd, it is essential to mention that, since Pd$3d_{5/2}$ overlaps with Au$4d_{5/2}$, only Pd$3d_{3/2}$ absolute maxima must be considered, without further fitting,[42,43] in order to dispel any misgiving in the identification of Pd species. In this regard, and with the objective of having a trustworthy reference, **1.00Pd-H** was also analyzed after an *in situ* reduction at 200 ºC (Figure S5b). As in this catalyst the absence of gold allows for a correct analysis of the Pd$3d_{5/2}$ line, which mainly corresponds to Pd^0, it is possible to establish its Pd$3d_{3/2}$ absolute maxima, centered at 341.1 eV, as a good indicator of a sample mainly containing Pd^0 species. Following this, Figure 4a shows how **0.8Pd-0.2Au-H** and **1.00Pd-H**, with binding energy values for Pd$3d_{3/2}$ of 342.0 and 342.1 eV, present an important contribution of oxidized palladium species.

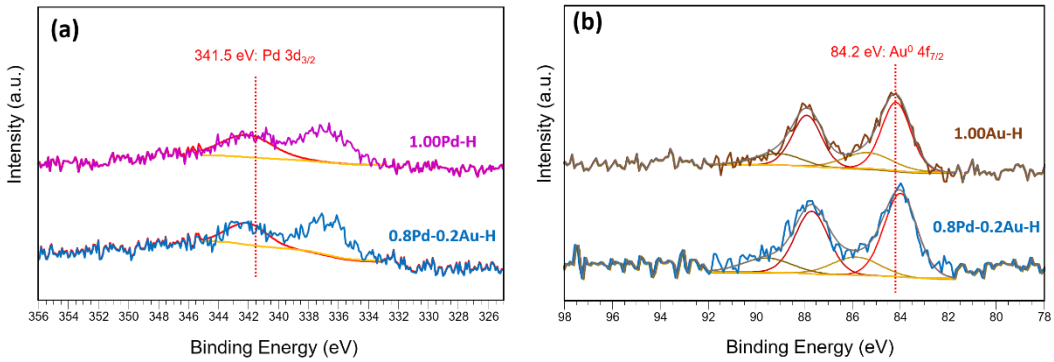

Figure 4. XPS spectra of (a) Pd3*d* after analyzing only the Pd3$d_{3/2}$ maxima and (b) Au4*f* after peak fitting.

As for Pd, in Figure 4b, **1.00Au-H**, and **0.8Pd-0.2Au-H** present mainly metallic Au (84.2-84.0 eV) and a smaller proportion of $Au^{\delta+}$ (85.3-85.9 eV).[44] However, a small negative shift of 0.2 eV can be observed in this sample containing Pd for Au$4f_{7/2}$ line of Au^0 (**0.8Pd-0.2Au-H)** being the B.E. 84.0 vs 84.2 eV for **1.00Au-H**. Although too small as to be totally reliable, this shift might be another proof of the formation of the desired Pd-Au alloy, since it has been stated that there is a net charge flowing into Au as a consequence of its electronic modification when alloying with Pd.[45,46] Nonetheless, either initial state effects resulting from H_2 pretreatment,[47] or electron transfer from the support to the nanoparticles may also account for this shift.[48]

3.3 Activity-structure correlation for aerobic of benzyl alcohol oxidation

In order to correlate the catalytic activity with the catalyst structure, the first fact that should be discussed is the synthetic method. Materials in which metal precursors were reduced with hydrogen instead of sodium borohydride led to higher activity than those compositionally equivalent but using borohydride as a reducing agent. According to the previous STEM observations, this behavior can easily be related to the nanoparticle size and dispersion on the support. Indeed, in the case of **0.2Pd-0.8Au-NBH**, the nanoparticles are poorly dispersed and much bigger in terms of size when compared with its equivalent **0.2Pd-0.8Au-H**, prepared under a H_2 flow. This leads to a drastic decrease in the active area with respect to the catalyst prepared with the thermal method herein described (**0.2Pd-0.8Au-H**), a fact clearly verified by CO-chemisorption measurements (2.9 vs 7.4 µmol CO/g, Table S1). Additionally, the Pd/Au ratio affects the active phase dispersion strongly. In fact, CO-chemisorption shows a higher dispersion and, therefore, a higher amount of active phase exposed in the case of **0.8Pd-0.2Au-H** than for **0.2Pd-0.8Au-H** (15.4 vs 7.4 µmol CO/g).

To sum up, at this point, there seems to be a positive synergy between Pd and Au for the benzyl alcohol conversion, where the metal ratio of bimetallic nanoparticles plays an important role

in it, thereby affecting the catalyst performance in this catalytic reaction. Additionally, better dispersion and smaller particle size (higher active surface area) induced by the hydrogen reduction step, and likely to be dependent on the Au/Pd molar ratio as well, are also essential points to developing an efficient heterogeneous catalyst for this selective primary alcohol oxidation.

3.4 Kinetic studies on benzyl alcohol oxidation

From this point onwards, various kinetic studies will be discussed in order to obtain a better understanding of the catalyst behavior in the reaction under study. According to all kinetics, several points must be remarked: first, as seen in Figure S7, catalysts reduced by dihydrogen appear to have a necessary induction step. Although the reaction directly starts, a rise of activity is noticed after a few hours of reaction. To ascertain whether PdO formation could be the cause of this induction time, a commercial palladium oxide catalyst was tested in reaction, giving 0% conversion and thereby discarding PdO to be the active species for this reaction.

Another important point concerns selectivity. Each catalyst is selective to the aldehyde up to a certain extent. In this sense, it appears that catalysts prefer to react firstly with the alcohol, but when the concentration of aldehyde starts to be high, catalysts also react with the aldehyde to give the corresponding carboxylic acid. In this sense, and to test the affinity to react with either aldehyde or alcohol, a catalytic reaction with only benzaldehyde as reagent was carried out under the same conditions with catalyst **0.8Pd-0.2Au-H,** and a conversion of 8% benzaldehyde to benzoic acid was observed. This result confirms that, although not totally selective, the catalyst is not particularly good at oxidizing aldehydes. Indeed, according to the literature, the selectivity is induced by the reactant and not by the catalyst.[49] In an aqueous solution, the selectivity is brought by a primary hydroxyl group located next to an aromatic ring. With this configuration, the aldehyde form is stabilized by conjugation. Therefore, the carboxylic acid formation is more challenging than it would be for an aliphatic alcohol, for example.

Overall, Figure S7 shows how, in good agreement with what has been discussed before (Table 2), **0.8Pd-0.2Au-H** is the most promising one, since it allows for keeping the highest level of selectivity when working at a very high conversion.

Afterwards, to evaluate catalyst activity and selectivity easily, TON and TOF in different conditions were calculated and compared with each other (Table 3). In this case, only those materials prepared by using the hydrogen reduction pathway and with different Pd/Au ratios in the nanoparticles were assessed. In this sense, two comparison ways were adopted. Firstly, TOF were compared at the same conversion to classify the different catalysts in terms of their activity per Pd centre. Then, TONs at the highest selectivity and conversion level in each case

were compared to determine the best compromise to success in our aim. As for the former comparison, considering a conversion equal to 25% and 100% of selectivity, the best TOF is obtained with **0.5Pd-0.5Au-H**. This means that increasing the amount of gold induces an improvement in the catalyst activity, which is, according to the kinetic curves, likely to be related to a decrease in the induction step. In other words, to achieve a 25% conversion with 100% selectivity, **0.5Pd-0.5Au-H** (with the largest amount of gold) is the fastest and, therefore, the most active catalyst. However, considering the highest conversion with 100% of selectivity, the discussion is different. Although **0.5Pd-0.5Au-H** remains the most active catalyst (see Figure S7), for the same selectivity (100%), a better conversion is obtained with **0.8Pd-0.2Au-H**. In this case, the TON is higher when it is compared at the highest selectivity level. Thus, **0.8Pd-0.2Au-H** keeps the right balance between activity and selectivity to obtain benzaldehyde in more significant amounts, which could be associated with a better particle size distribution in this last case (Figure 2). Furthermore, the TOF comparison and the kinetic results reported in Figure S7 also confirm that this catalyst 0**.8Pd-0.2Au-H** can achieve this performance (i.e., almost quantitative yields to benzaldehyde) in shorter reaction times than 1.00Pd-H.

Table 3. TON and TOF of different catalysts.

Catalysts	Conversion = 25%, Selectivity = 100%	Highest Conversion with a selectivity = 100%	
	TOF (h^{-1})	Conversion (%)	TON
1.00Pd-H	32	84	420
0.8Pd-0.2Au-H	50	94	465
0.5Pd-0.5Au-H	104	80	400
0.2Pd-0.8Au-H	31	53	265

Reaction conditions: [benzyl alcohol] = 0.3 M, alcohol/metal ratio: 500/1 mol, 60 °C, 1.5bar O_2

Up to now, the discussion led to choosing **0.8Pd-0.2Au-H** as the system keeping the right balance between activity and selectivity to converting a primary aryl-alcohol to an aryl-aldehyde in a selective way. Consequently, catalyst stability was tested by conducting a reusability study whereby the catalyst was used several times in the same reaction. Figure 5 shows the result of these experiments. A slight increase in conversion and a slight decrease in selectivity might occur throughout the different catalytic cycles. Remarkably, according to the STEM results (Figure 2g, 5c and 5d), no agglomeration after catalysis has been detected, and nanoparticle size distribution is still similar before and after catalysis, so the material seems to be very stable. Additionally, an ICP analysis of the reaction mixture (after catalyst filtration) was

recorded to verify this observation. No traces of any metal were found. These two analyses dismiss the leaching of nanoparticles during the process. To further study this, a kinetic study of a reused catalyst was carried out, resulting in the disappearance of the induction time (Figure 5a). By and large, the catalyst has the same behavior until the fourth use, appearing to be very stable.

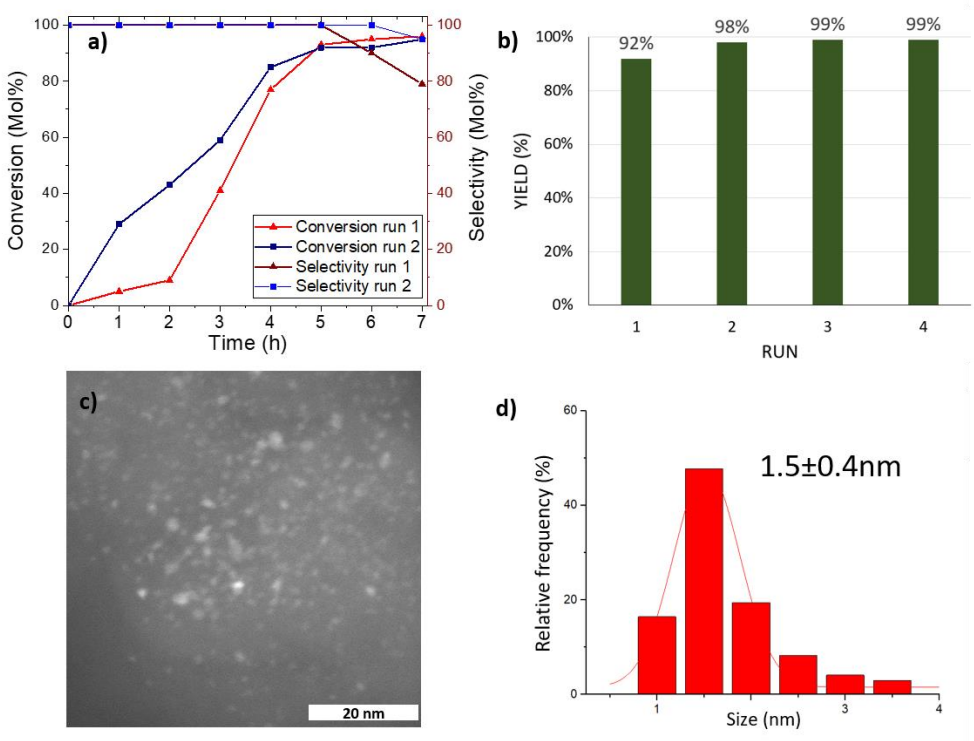

Figure 5. a) Conversion and selectivity depending on time for **0.8Pd-0.2Au-H** at the first and second run, b) reusability of the **0.8Pd-0.2Au-H** on benzyl alcohol oxidation. c) TEM image of **0.8Pd-0.2Au-H after reaction** and d) the corresponding particle size distribution. Reaction conditions: [benzyl alcohol] = 0.3 M, alcohol/metal ratio: 500/1 mol, 60 °C, 1.5 bar O_2, 5 h (for reuses).

Additionally, XPS analysis of **0.8Pd-0.2Au-H** and **0.8Pd-0.2Au-H after reaction** were compared to confirm the stability of the material during the catalytic process (Figure S6). The shift towards lower binding energy for Pd$3d_{3/2}$; 341.6 eV, in the case of **0.8Pd-0.2Au-H after reaction** indicates a material with a more considerable amount of Pd^0 on its surface. Excitingly, this enrichment in Pd^0 could explain the disappearance of the induction time in the reused catalyst. However, this slight stabilization of Pd^0 throughout the reaction cannot be attributed to the presence of Au since **1.00Pd-H after reaction**, with only Pd, also presents a low value for $Pd3d_{3/2}$ (341.5 eV). As for Au, **0.8Pd-0.2Au-H after reaction** still presents mainly metallic Au (84.2-84.0 eV) and a small proportion of $Au^{\delta+}$ (85.3-85.9 eV).

3.5. H_2O_2 Production and Benzyl alcohol oxidation

Preliminary results of benzyl alcohol oxidation testing different oxidants have shown that catalysts **0.8Pd-0.2Au-H** and **0.5Pd-0.5Au-H** provide the best activities when employing a mixture of O_2 and H_2O_2 (Table S3). Interestingly, in the literature, supported PdAu nanoparticles are often reported as promising catalysts for H_2O_2 synthesis, Au incorporation being responsible for an enhancement in H_2O_2 selectivity with respect to the corresponding Pd systems.[50,51] Although still widely debated in the literature, with electronic, structural and isolation effects as potential causes for the enhancement, several theoretical and experimental studies provided evidence that the presence of Au inhibits the formation of H_2O, the surface composition of Au−Pd catalysts being essential to determine O−O bond dissociation and, therefore, H_2O formation.[52,53]

Therefore, H_2O_2 production from H_2 and O_2 was evaluated with several Pd-Au-H systems with and without benzyl alcohol for 2 hours at 0 ºC (Figure S8). Remarkably, the presence of benzyl alcohol enhances the formation of H_2O_2 for the catalyst **0.5Pd-0.5Au-H**, while inhibits H_2O_2 production for the catalyst **0.8Pd-0.2Au-H** (Figure S8). Likely, adsorption of benzyl alcohol on **0.8Pd-0.2Au-H** catalyst reduces its capacity to activate oxygen to produce H_2O_2. In this regard, this was the most active catalyst for oxygen activation in aerobic oxidation of benzyl alcohol. On the other side, the adsorption of this alcohol on a gold-richer catalyst **0.5Pd-0.5Au-H** might reduce its activity to decompose H_2O_2. In fact, it is well known that pure gold catalysts are prone to peroxide decomposition[49] and, indeed, this was the most active catalyst for oxidation employing H_2O_2, which directly implies decomposition of H_2O_2 to O_2 and water.

Based on that, we decided to carry out the same experiment but increasing the temperature to 60 ºC after 2 hours in order to couple and evaluate the H_2O_2 production and benzyl alcohol oxidation (Figure 6, Table S4). Both catalysts were active for the aerobic oxidation, but catalyst **0.5Pd-0.5Au-H** was the best when employing H_2O_2 as oxidant (Table S3). However, for the tandem process, both H_2O_2 production (with and without the alcohol at the beginning) at 0 ºC and subsequent benzyl alcohol oxidation at 60 ºC, catalyst **0.8Pd-0.2Au-H** shows the best results, with conversion higher than 60% and good selectivity to aldehyde, being a more suitable catalyst for this tandem strategy. The better results obtained with this catalyst could be related to the higher O_2 pressure (10 bar at initial point), since it has shown excellent activity for aerobic oxidation (Table 1). This effect is also reflected in a lower selectivity versus the reaction with a pressure of 1.5 bar O_2. This would indicate that aerobic oxidation controls this process versus oxygen transfer from H_2O_2. Finally, the spent catalyst has been analyzed by STEM and TEM microscopy and the corresponding NP size distribution is presented in Figure

S13. The used catalyst presents average size nanoparticles of 1.4±0.7nm. **0.8Pd-0.2Au-H after the tandem process** seems to be a robust catalyst despite a slight increase in the standard deviation of the average nanoparticle size compared to before the reaction.

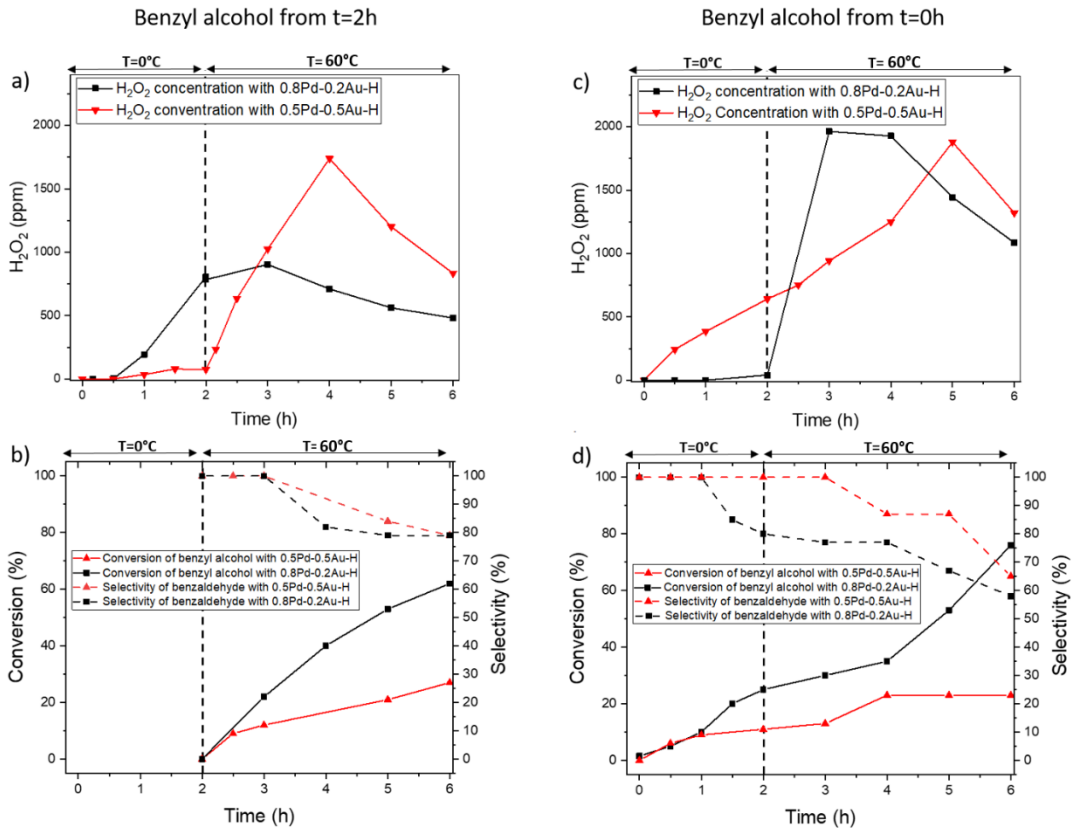

Figure 6. a) Hydrogen peroxide production and b) benzyl alcohol oxidation (t = 2h: temperature is up to 60 °C and benzyl alcohol is added) with **0.8Pd-0.2Au-H** and **0.5Pd-0.5Au-H** as catalysts and c) Hydrogen peroxide production and d) benzyl alcohol oxidation (t = 2h: temperature is up to 60 °C but benzyl alcohol has been added at t = 0h) with **0.8Pd-0.2Au-H** and **0.5Pd-0.5Au-H** as catalysts. Reaction conditions: H_2O as solvent, benzyl alcohol: 100 µL, alcohol/metal ratio: 750/1 mol, 10 bar O_2, 10 bar H_2, 20 bar CO_2.

4. Conclusions

Two strategies were used in this work to develop carbon-supported Pd-Au bimetallic nanoparticles. In this sense, XRD, XPS and EDX analyses provide compelling evidence for the bimetallic character of the nanoparticles presented herein. The "traditional" pathway involves sodium borohydride as a reductive agent for metal precursors. The other pathway, considered more environmentally friendly and much more straightforward, consists of a reduction step of metal precursors under a dihydrogen flow at 200 °C, for 2h. Both methods

were used to obtain bimetallic materials in different compositional ranges. Likewise, the resulting materials have been tested and studied in the aryl-alcohol oxidation, and their catalytic activity has been correlated with their physical properties.

On the one hand, the materials prepared via the hydrogen reduction process exceed the catalytic results for those materials synthesized with the "traditional" method by inducing a higher metal dispersion of the catalysts thereby attained. On the other hand, the palladium-gold ratio also plays an essential role in the metal dispersion, thus improving the one observed for the monometallic ones. Therefore, this metal dispersion seems to be a key point defining the optimum synergy between the two metals. According to XPS results, the nature of this positive synergy between Pd and Au might also come from a different electronic structure when both metals are present and close enough to interact.

Concretely, **0.8Pd-0.2Au-H** brings the best compromise to selectively convert a primary alcohol into an aldehyde without overoxidation to the carboxylic acid. This leads to a more active material showing high stability over several catalytic cycles. Furthermore, considering that this catalyst has shown an interesting activity for H_2O_2 production at 0 ºC, a tandem process for H_2O_2 production coupled with benzyl alcohol oxidation has been carried out with high conversion and moderate selectivity towards benzaldehyde.

In summary, the results obtained in this work should further strengthen the confidence in PdAu bimetallic systems prepared by a simple hydrogen reduction step as an alternative tool to design nanoparticle-based catalytic systems presenting an enhanced activity in the selective benzyl oxidation to benzaldehyde and for tandem processes involving H_2O_2 production.

Declaration of Competing Interest

The authors declare no competing financial interest.

Acknowledgment

Authors thank the financial support by the Spanish Government (RTI2018-096399-A-I00 and PGC2018-097277-B-I00 funded by MICINN/AEI/ 10.13039/501100011033) and Junta de Andalucía (P20 01027 and PYC 20 RE 060 UAL). The Electron Microscopy Service of the UPV is acknowledged for their help in sample characterization.

Appendix A. Supporting information

Detailed catalysts synthesis, additional characterization data, kinetic studied and detailed catalytic results are available in the Supporting Information of this article.

References

1 A. Savara, C. E. Chan-Thaw, I. Rossetti, A. Villa and L. Prati, *ChemCatChem*, 2014, **6**, 3464–3473.

2 C. Della Pina, E. Falletta and M. Rossi, *J. Catal.*, 2008, **260**, 384–386.

3 M. Besson and P. Gallezot, *Catal. Today*, 2000, **57**, 127–141.

4 Z. qiang Lei and R. ren Wang, *Catal. Commun.*, 2008, **9**, 740–742.

5 S. Biella and M. Rossi, *Chem. Commun.*, 2003, 378–379.

6 V. R. Choudhary, P. A. Chaudhari and V. S. Narkhede, *Catal. Commun.*, 2003, **4**, 171–175.

7 S. ya Fujibayashi, K. Nakayama, M. Hamamoto, S. Sakaguchi, Y. Nishiyama and Y. Ishii, *J. Mol. Catal. A Chem.*, 1996, **110**, 105–117.

8 D. Feng, Y. Dong, L. Zhang, X. Ge, W. Zhang, S. Dai and Z. Qiao, *Angew. Chemie*, 2020, **132**, 19671–19677.

9 H. Ji, K. Ebitani, T. Mizugaki and K. Kaneda, *React. Kinet. Catal. Lett.*, 2003, **78**, 73–80.

10 F. Gao and D. W. Goodman, *Chem. Soc. Rev.*, 2012, **41**, 8009–8020.

11 A. Savara, C. E. Chan-Thaw, J. E. Sutton, D. Wang, L. Prati and A. Villa, *ChemCatChem*, 2017, **9**, 253–257.

12 C. E. Chan-Thaw, A. Savara and A. Villa, *Catalysts*, 2018, **8**, 1–21.

13 A. Santos, R. J. Lewis, G. Malta, A. G. R. Howe, D. J. Morgan, E. Hampton, P. Gaskin and G. J. Hutchings, *Ind. Eng. Chem. Res.*, 2019, **58**, 12623–12631.

14 A. Paul, L. M. D. R. S. Martins, A. Karmakar, M. L. Kuznetsov, A. S. Novikov, M. F. C. Guedes da Silva and A. J. L. Pombeiro, *J. Catal.*, 2020, **385**, 324–337.

15 A. T. J. Zhu, K, Kailasam, A. Fischer, *ACS Catal.*, 2011, **1**, 342–347.

16 F. Galvanin, M. Sankar, S. Cattaneo, D. Bethell, V. Dua, G. J. Hutchings and A. Gavriilidis, *Chem. Eng. J.*, 2018, **342**, 196–210.

17 X. Li, J. Feng, M. Perdjon, R. Oh, W. Zhao, X. Huang and S. Liu, *Appl. Surf. Sci.*, 2020, **505**, 144473.

18 Z. Wang, J. Feng, X. Li, R. Oh, D. Shi, O. Akdim, M. Xia, L. Zhao, X. Huang and G. Zhang, *J. Colloid Interface Sci.*, 2021, **588**, 787–794.

19 M. Chen, D. Kumar, C. W. Yi and D. W. Goodman, *Science*, 2005, **310**, 291–293.

20 C. M. Crombie, R. J. Lewis, R. L. Taylor, D. J. Morgan, T. E. Davies, A. Folli, D. M. Murphy, J. K. Edwards, J. Qi, H. Jiang, C. J. Kiely, X. Liu, M. S. Skjøth-Rasmussen and G. J. Hutchings, *ACS Catal.*, 2021, **11**, 2701–2714.

21 Y. Nomura, T. Ishihara, Y. Hata, K. Kitawaki, K. Kaneko and H. Matsumoto, *ChemSusChem*, 2008, **1**, 619–621.

22 I. Moreno, N. F. Dummer, J. K. Edwards, M. Alhumaimess, M. Sankar, R. Sanz, P. Pizarro, D. P. Serrano and G. J. Hutchings, *Catal. Sci. Technol.*, 2013, **3**, 2425–2434.

23 M. Santonastaso, S. J. Freakley, P. J. Miedziak, G. L. Brett, J. K. Edwards and G. J. Hutchings, *Org. Process Res. Dev.*, 2014, **18**, 1455–1460.

24 P. Gallezot, *Catal. Today*, 1997, **37**, 405–418.

25 N. Dimitratos, A. Villa, C. L. Bianchi, L. Prati and M. Makkee, *Appl. Catal. A Gen.*, 2006, **311**, 185–192.

26 N. Dimitratos, A. Villa, D. Wang, F. Porta, D. Su and L. Prati, *J. Catal.*, 2006, **244**, 113–121.

27 Casa XPS. Software Ltd, .

28 S. Carrettin, P. McMorn, P. Johnston, K. Griffin, C. J. Kiely, G. A. Attard and G. J. Hutchings, *Top. Catal.*, 2004, **27**, 131–136.

29 J. Han, Y. Liu and R. Guo, *Adv. Funct. Mater.*, 2009, **19**, 1112–1117.

30 X. Yu, Y. Huo, J. Yang, S. Chang, Y. Ma and W. Huang, *Appl. Surf. Sci.*, 2013, **280**, 450–455.

31 T. Mallat and A. Baiker, *Chem. Rev.*, 2004, **104**, 3037–3058.

32 G. Nagy, A. Beck, G. Sáfrán, Z. Schay, S. Liu, T. Li, B. Qiao, J. Wang and K. Lázár, *React. Kinet. Mech. Catal.*, 2019, **128**, 71–95.

33 E. V. Shtykova, D. I. Svergun, D. M. Chernyshov, I. A. Khotina, P. M. Valetsky, R. J. Spontak and L. M. Bronstein, *J. Phys. Chem. B*, 2004, **108**, 6175–6185.

34 A. R. Denton and N. W. Ashcroft, *Phys. Rev. A*, 1991, **43**, 3161.

35 G. Zhang, H. Zhou, C. An, D. Liu, Z. Huang and Y. Huang, *Colloid Polym. Sci.*, 2012, **290**, 1435–1441.

36 H. Miura, K. Endo, R. Ogawa and T. Shishido, *ACS Catal.*, 2017, **7**, 1543–1553.

37 U. Holzwarth and N. Gibson, *Nat. Nanotechnol.*, 2011, **6**, 534–534.

38 L. M. Rivera Gavidia, G. García, D. Anaya, A. Querejeta, F. Alcaide and E. Pastor, *Appl. Catal. B Environ.*, 2016, **184**, 12–19.

39 B. Ledesma, J. Juárez, J. Mazarío, M. Domine and A. Beltramone, *Catal. Today*, 2021, **360**, 147–156.

40 G. Greczynski and L. Hultman, *Prog. Mater. Sci.*, 2020, **107**, 100591.

41 G. V. Zhutaeva, V. A. Bogdanovskaya, E. S. Davydova, L. P. Kazanskii and M. R. Tarasevich, *J. Solid State Electrochem.*, 2014, **18**, 1319–1334.

42 J. Xu, T. White, P. Li, C. He, J. Yu, W. Yuan and Y. F. Han, *J. Am. Chem. Soc.*, 2010, **132**, 10398–10406.

43 J. Liu, J. Shan, F. R. Lucci, S. Cao, E. C. H. Sykes and M. Flytzani-Stephanopoulos, *Catal. Sci. Technol.*, 2017, **7**, 4276–4284.

44 M. P. Casaletto, A. Longo, A. Martorana, A. Prestianni and A. M. Venezia, *Surf. Interface Anal.*, 2006, **38**, 215–218.

45 T. S. Chou, M. L. Perlman and R. E. Watson, *Phys. Rev. B*, 1976, **14**, 3248.

46 P. A. P. Nascente, S. G. C. De Castro, R. Landers and G. G. Kleiman, *Phys. Rev. B*, 1991, **43**, 4659.

47 J. Radnik, C. Mohr and P. Claus, *Phys. Chem. Chem. Phys.*, 2003, **5**, 172–177.

48 S. Arrii, F. Morfin, A. J. Renouprez and J. L. Rousset, *J. Am. Chem. Soc.*, 2004, **126**, 1199–1205.

49 J. Muzart, *Tetrahedron*, 2003, **59**, 5789–5816.

50 J. K. Edwards, B. E. Solsona, P. Landon, A. F. Carley, A. Herzing, C. J. Kiely and G. J. Hutchings, *J. Catal.*, 2005, **236**, 69–79.

51 B. E. Solsona, J. K. Edwards, P. Landon, A. F. Carley, A. Herzing, C. J. Kiely and G. J. Hutchings, *Chem. Mater.*, 2006, **18**, 2689–2695.

52 J. Li and K. Yoshizawa, *Catal. Today*, 2015, **248**, 142–148.

53 T. Ricciardulli, S. Gorthy, J. S. Adams, C. Thompson, A. M. Karim, M. Neurock and D. W. Flaherty, *J. Am. Chem. Soc.*, 2021, **143**, 5445–5464.